Electronic Supplementary Information

Stimuli Responsive and Reversible Crystalline-Amorphous Transformation in a Molecular Solid: Fluorescence Switching and Enhanced Phosphorescence in the Amorphous State

Pagidi Sudhakar* and T. P. Radhakrishnan*

School of Chemistry, University of Hyderabad, Hyderabad – 500 046, India

E-mail: tpr@uohyd.ac.in

Contents

Spectral Characterizations

NMR Spectra

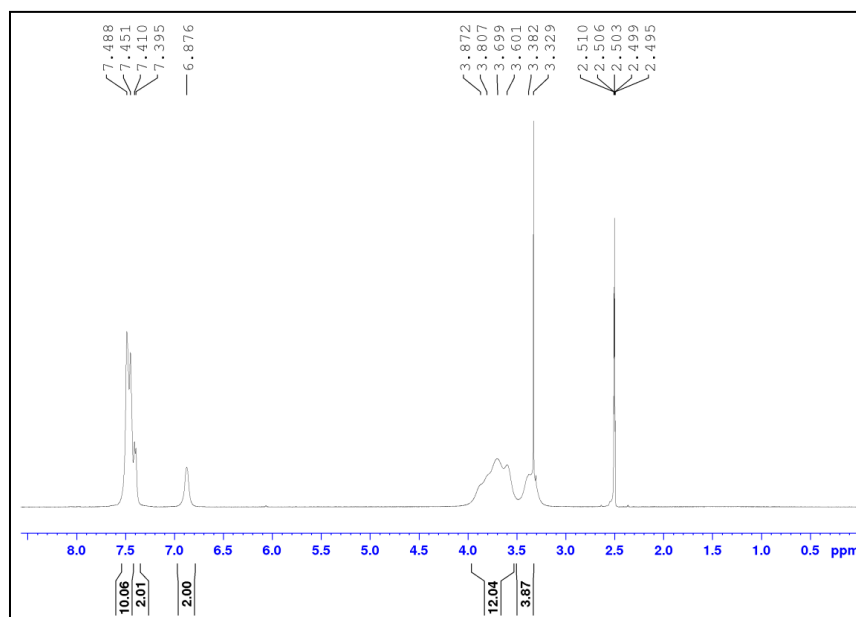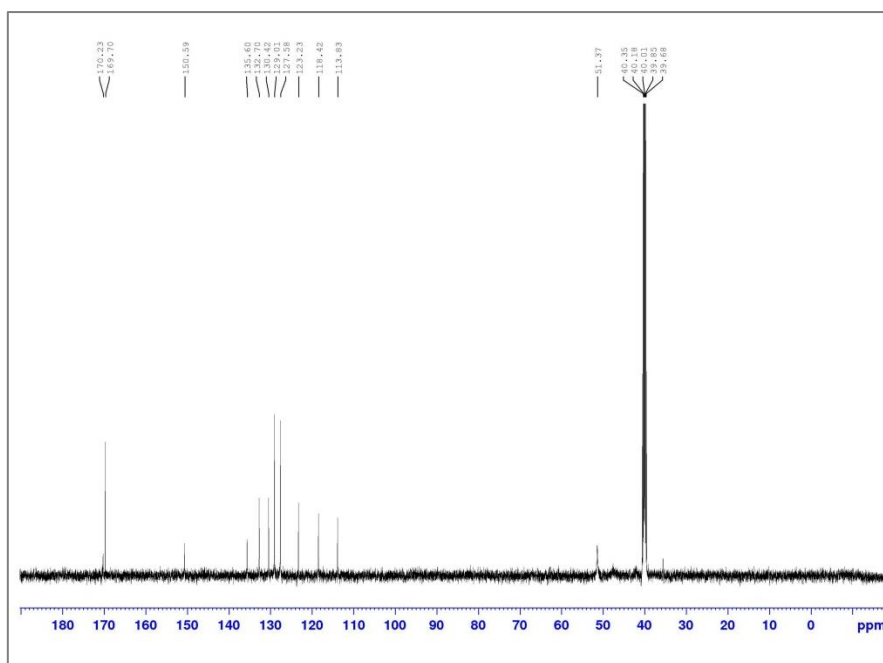**Figure S1.** ^{1}H NMR spectrum of BBPDQ.

Figure S2. ^{13}C NMR spectrum of BBPDQ.
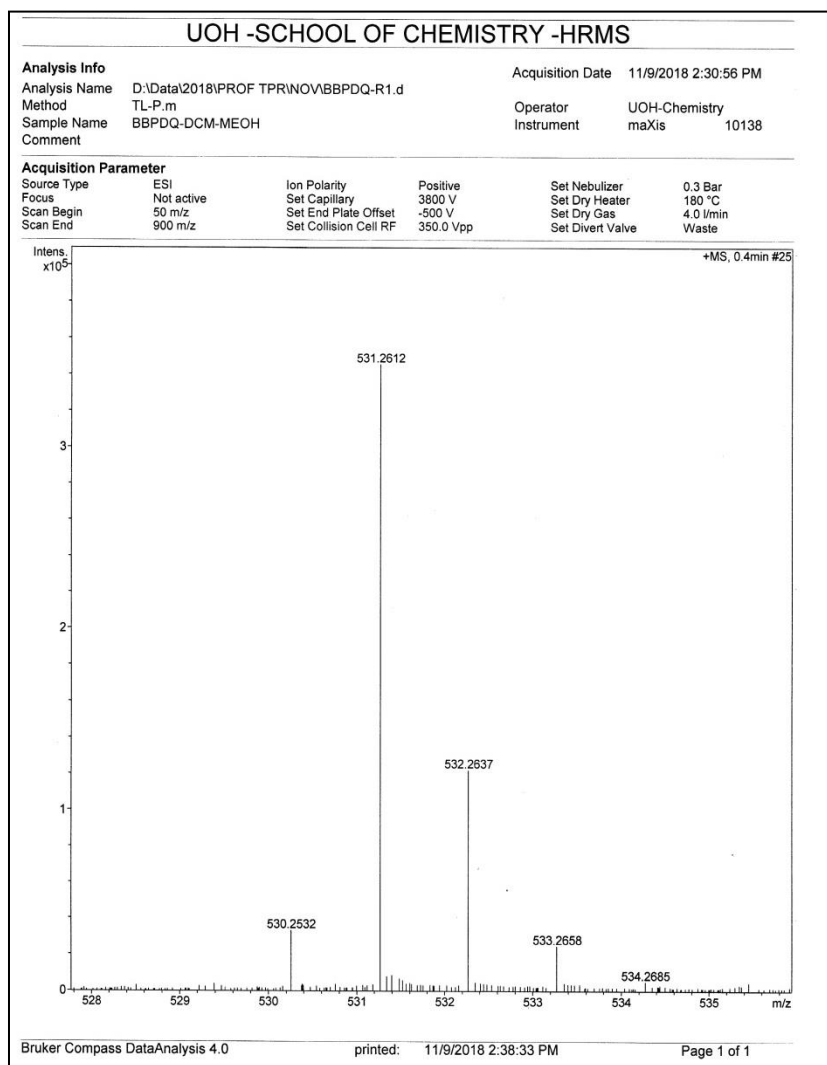
Mass spectrum

Figure S3. High resolution mass spectrum of BBPDQ.

Crystallographic Data

**Table S1.** Crystallographic data for BBPDQ; structure of the asymmetric unit is shown.

Molecule	BBPDQ.CH$_2$Cl$_2$
Empirical formula	C$_{33}$ H$_{32}$ Cl$_2$ N$_6$ O$_2$
Formula weight	615.54
Temperature(K)	297(2)
Wavelength (Å)	0.71073
Crystal system	Orthorhombic
Space group	*P2$_1$2$_1$2$_1$*
a/ Å	10.6483(5)
b/ Å	13.2218(6)
c/ Å	22.2843(9)
α/°	90
β/°	90
γ/°	90
V/Å^3	3137.4(2)
Z	4
Density(g cm^{-3})	1.303
Final R [I > 2σ$_I$]	R1 = 0.0708, wR2 = 0.1875
R (all data)	R1 = 0.1070, wR2 = 0.2068
Highest Peak(e.Å^{-3})	0.565
Deepest Hole (e.Å^{-3})	-0.590
Collected reflns	80266
Unique reflns	5522
No. of parameters	388
Theta range for data collection	2.39 to 25.0
Absorption coefficient (mm^{-1})	0.247
Goodness-of-fit on F^2	1.035
CCDC No.	1881774
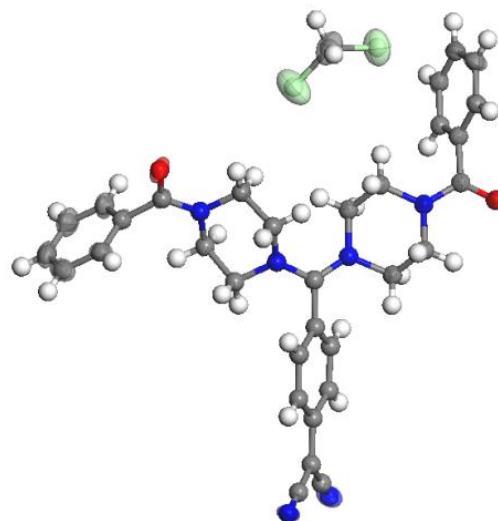
Spectroscopic Studies

Table S2. Photophysical properties of BBPDQ; the absorption maximum wavelength (λ_{abs}), fluorescence maximum wavelength (λ_{em}) and Stokes shifts ($\Delta\nu_{ST}$) are shown.

Solvent	λ_{abs} (nm)	λ_{em} (nm)	$\Delta\nu_{ST}$ (cm^{-1})
Dichloromethane	478	555	2902
Ethyl acetate	468	542	2917
Acetone	442	539	4072
Acetonitrile	432	536	4492
Dimethyl sulfoxide	429	528	4371
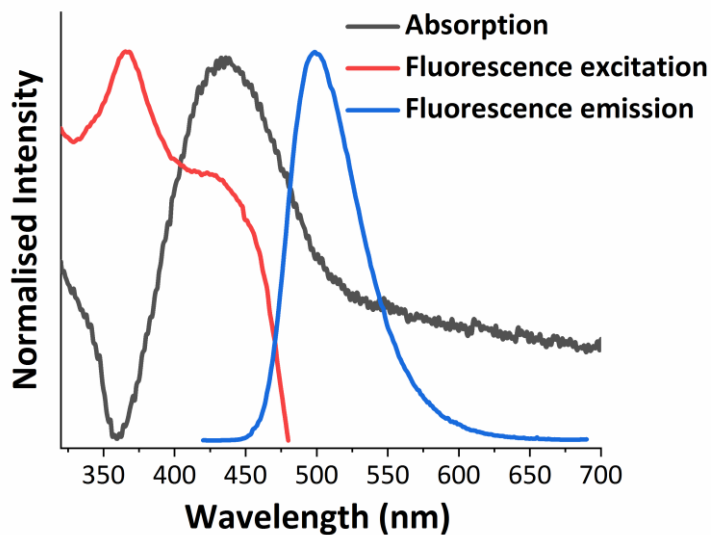
Figure S4. Absorption, emission (λ_{exc} = 350 nm) and excitation (λ_{em} = 498 nm) spectra of microcrystalline BBPDQ.
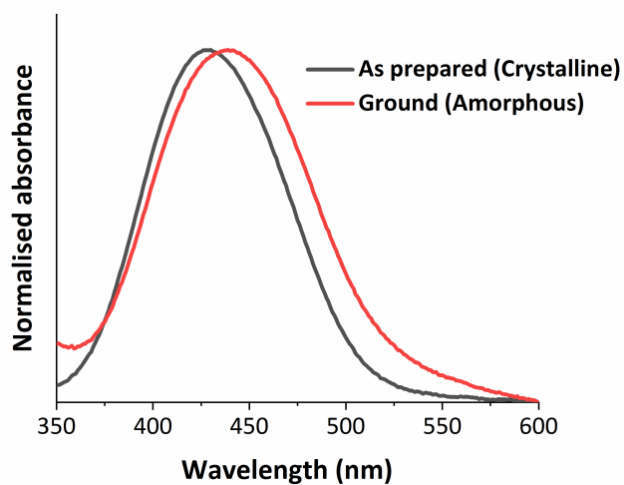
Figure S5. Absorption of as prepared and ground form of BBPDQ.
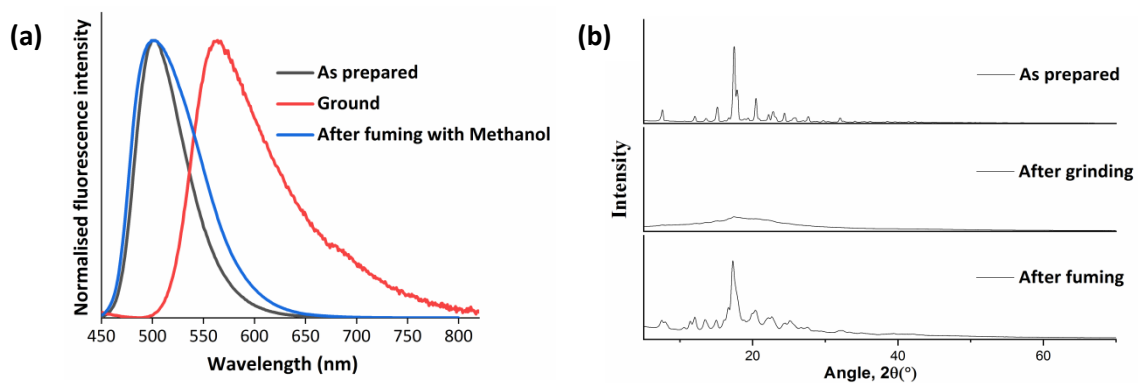
Figure S6. (a) Fluorescence emission (λ_{exc} = 350 nm) spectra of BBPDQ, as-prepared, mechanically ground, and solvent (methanol) fumed. **(b)** Powder X-ray diffraction patterns of BBPDQ samples: microcrystalline, mechanically ground and methanol fumed.
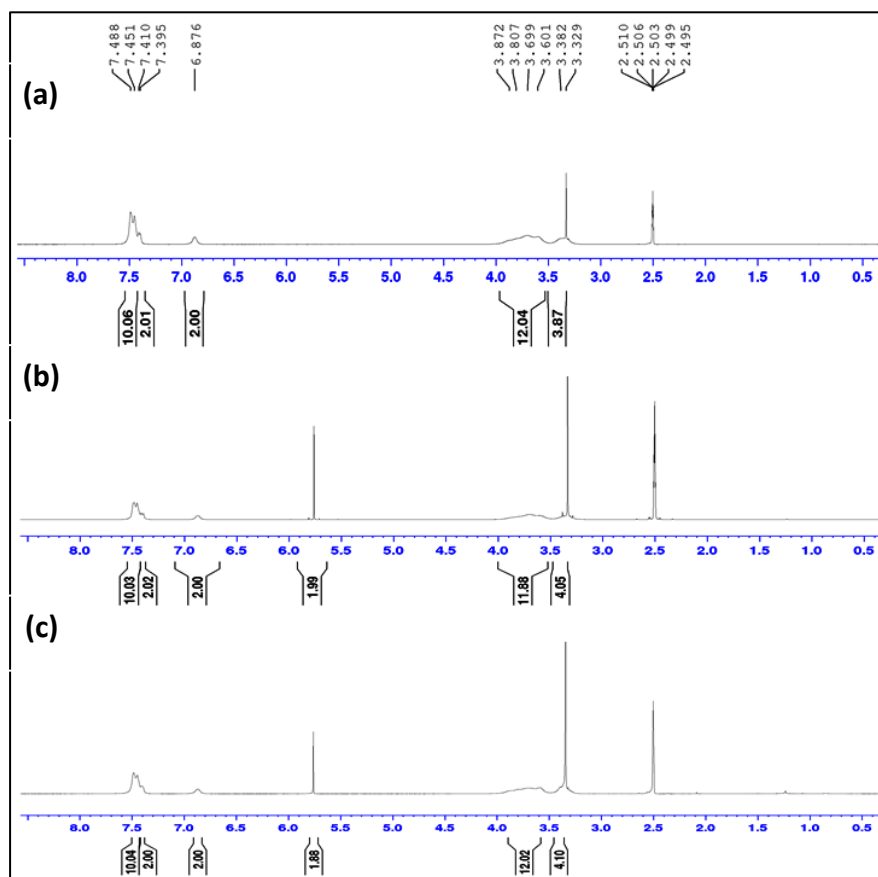
Figure S7. ^{1}H NMR spectra of BBPDQ: **(a)** pure material directly from the synthesis, **(b)** recrystallized from dichloromethane, and **(c)** the ground material; the peak at δ = 5.76 ppm in (b) and (c) arise due to dichloromethane.
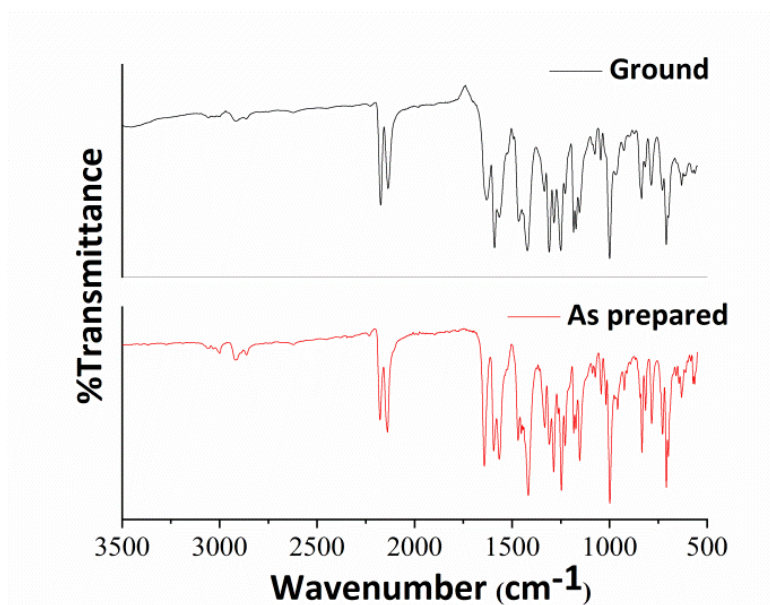
Figure S8. FT-IR spectra of the as prepared and ground forms of BBPDQ (selected region is shown in Fig. 4b).
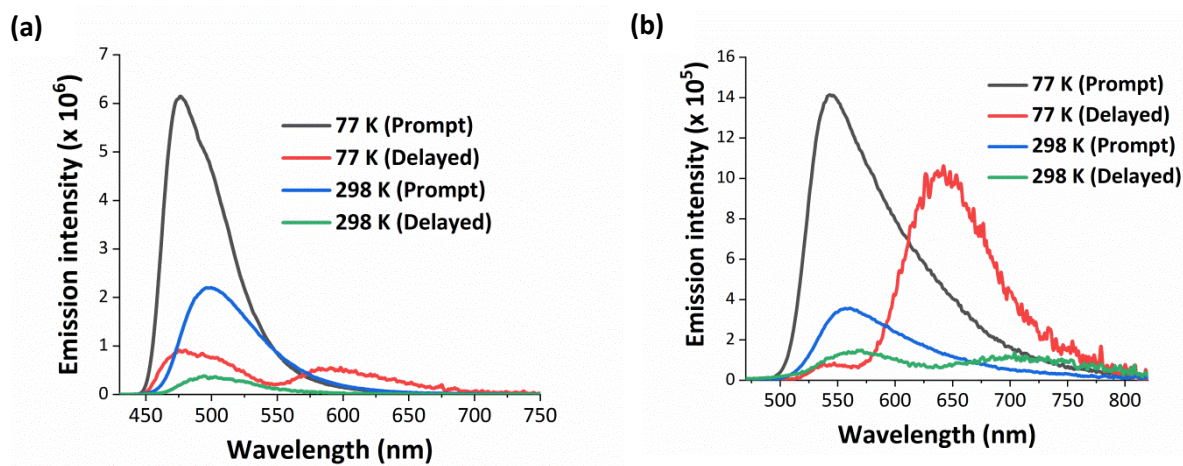
Figure S9. Prompt and delayed emission spectra (λ_{exc} = 350 nm) of **(a)** crystalline and **(b)** amorphous BBPDQ solid.
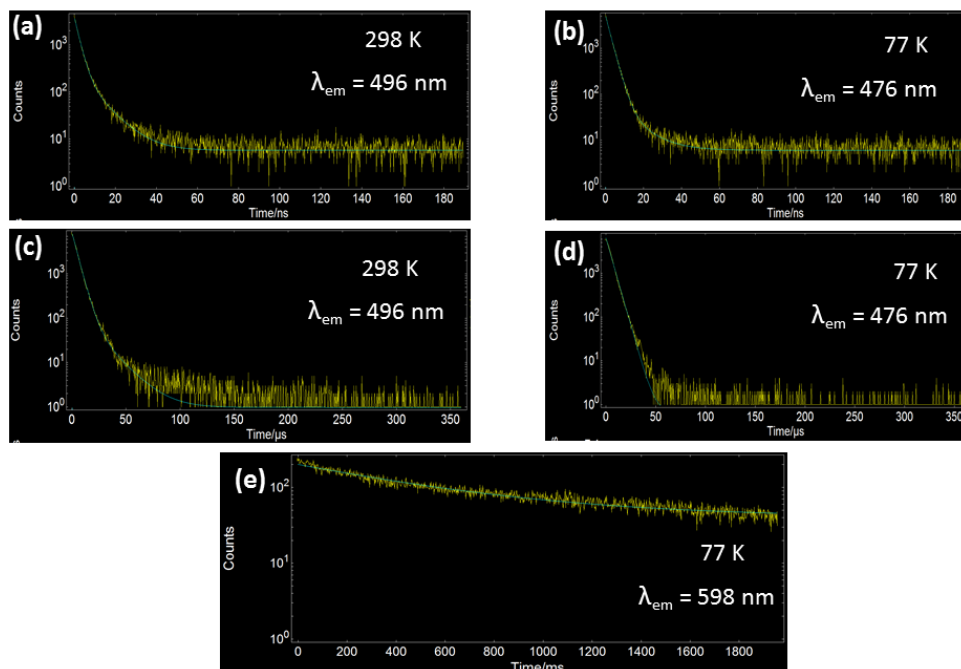
Figure S10. Prompt fluorescence decay profiles of crystalline BBPDQ at **(a)** 298 K and **(b)** 77 K; the fitting curves are shown. Delayed emission decay profiles of crystalline BBPDQ at **(c)** 298 K (at λ_{em} = 496 nm), **(d)** 77 K (at λ_{em} = 476 nm) and **(e)** 77 K (at λ_{em} = 598 nm) ; the fitting curves are shown.

Table S3: Emission lifetimes (individual components and average values) for crystalline BBPDQ at 298 K and 77 K [λ_{exc} = 350 nm for emission spectral measurements and 330 (nano-LED) for TCSPC measurements].

	λ_{em} (nm)	τ_1 (A_1)	τ_2 (A_2)	Mean lifetime	χ^2
298 K					
Prompt	496	2.45 ns (68 %)	10.04 ns (32%)	4.88 ns	1.18
Delayed	496	4.68 µs (95%)	17.77 µs (5%)	5.33 µs	1.09
77 K					
Prompt	476	2.56 ns (97 %)	13.25 ns (3%)	2.88 ns	1.18
Delayed	476	5.65 µs (100%)	-	5.65 µs	1.04
	598	575.71 ms (100 %)	-	575.71 ms	1.17
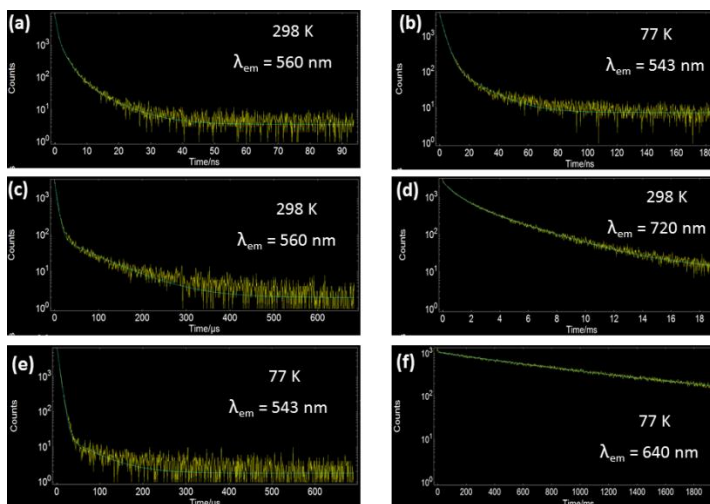
**Figure S11.** Prompt fluorescence decay profiles of amorphous BBPDQ at **(a)** 298 K and **(b)** 77 K; the fitting curves are shown. Delayed emission decay profiles of amorphous BBPDQ at **(c)** 298 K (at λ_{em} = 560 nm), **(d)** 298 K (at λ_{em} = 720 nm), **(e)** 77 K (at λ_{em} = 543 nm) and **(f)** 77 K (at λ_{em} = 640 nm); the fitting curves are shown.

Table S4. Emission lifetimes (individual components and average values) for amorphous BBPDQ at 298 K and 77 K [λ_{exc} = 350 nm for emission spectral measurements and 330 (nano-LED) for TCSPC measurements].

	λ_{em} (nm)	τ_1 (A$_1$)	τ_2 (A$_2$)	τ_3 (A$_3$)	Mean lifetime	χ^2
298 K						
Prompt	560	0.54 ns (34 %)	2.23 ns (48 %)	7.84 ns (17 %)	2.58 ns	1.17
Delayed	560	5.25 µs (87%)	57.83 µs (13 %)	-	12.08 µs	1.34
Delayed	715	857.32 µs (29 %)	3.46 ms (71 %)	-	2.71 ms	1.19
77 K						
Prompt	543	2.86 ns (79 %)	19.68 ns (21%)	-	6.39 ns	1.30
Delayed	543	5.56 µs (100 %)	-	-	5.56 µs	1.03
	640	979.93 ms (100 %)	-	-	979.93 ms	1.19

Table S5. The singlet-triplet ($S_1 \rightarrow T_1$) gap, ΔE_{ST} determined from the prompt and delayed emissions at 77K for BBPDQ.

Form	Transition	λ_{max}(nm) [eV]	ΔE_{ST} (eV)
Crystalline	$S_1 \rightarrow S_0$	476 [2.60]	0.53
	$T_1 \rightarrow S_0$	598 [2.07]	
Amorphous	$S_1 \rightarrow S_0$	543 [2.28]	0.34
	$T_1 \rightarrow S_0$	640 [1.94]	
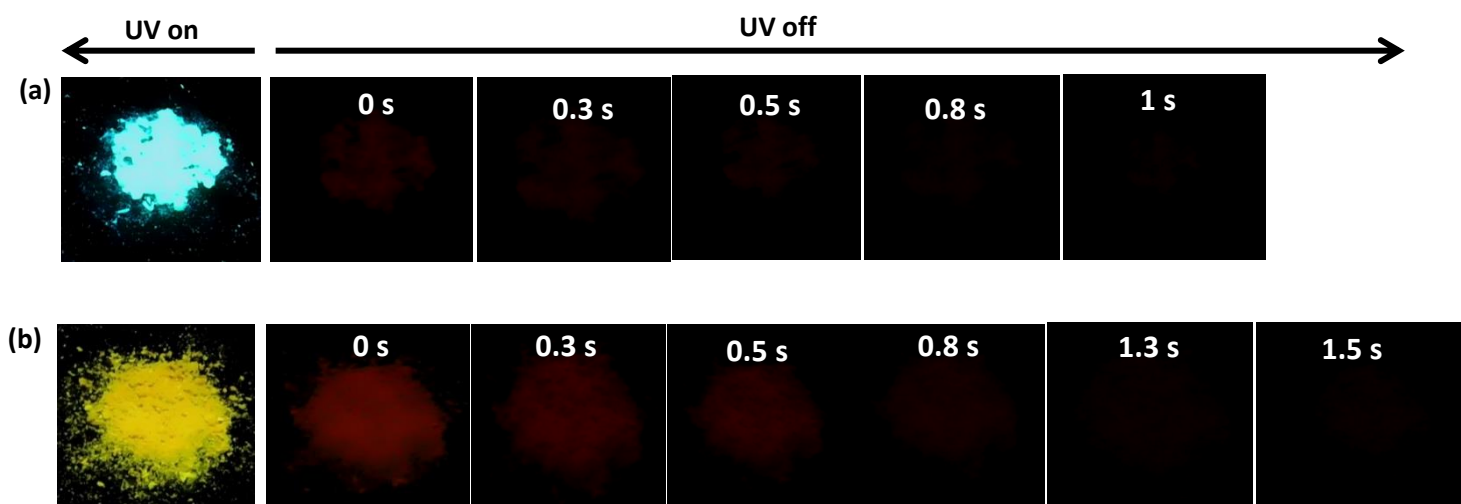
Figure S12. Photographs of **(a)** as prepared, and **(b)** ground form of BBPDQ (cooled by liquid N_2) under 365 nm UV light, and after switching off the UV irradiation.

Computational Studies

TD-DFT computations[S2] were carried out at the B3LYP/6-31G(d) level on the molecular geometry of BBPDQ taken from the crystal structure determination (Fig. S13), to estimate the electronic transition energies. The environment effect due to the polar neighboring molecules was modeled using the SCRF method; utility of this approach has been demonstrated in several earlier studies on DADQs.[S3] In addition to vacuum, two different solvents dichloromethane and acetonitrile were tried. The computed vertical transition energy in the case of dichloromethane (431 nm) is found to agree well with the experimental electronic absorption peak (432 nm) of the crystalline solid. Based on this observation, dichloromethane was chosen to mimic the molecular environment in the crystal; the vertical transition energy from the ground state (S_0) to the triplet (T_1) provides an estimate of the energy gap, ΔE_{ST}; the relevant data are provided in Table S6.
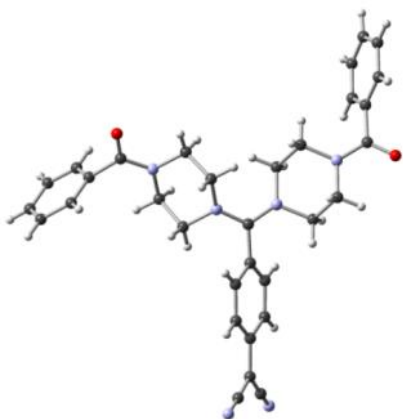

Figure S13. Molecular geometry of BBPDQ from crystal structure determination, used in the computation.

Table S6. Energies for the electronic transition from the ground electronic state (S_0) to the first excited singlet (S_1) and triplet (T_1) states, from the TD-DFT (B3LYP/6-31G(d)) computations including medium effect.

Medium	Transition	λ(nm) [eV]	f (oscillator strength)	ΔE_{ST} (eV)
Vacuum	$S_0 \rightarrow S_1$	469 [2.64]	0.7514	1.36
	$S_0 \rightarrow T_1$	967 [1.28]	-	
Dichloromethane	$S_0 \rightarrow S_1$	431 [2.87]	0.7887	0.85
	$S_0 \rightarrow T_1$	612 [2.02]	-	
Acetonitrile	$S_0 \rightarrow S_1$	416 [2.97]	0.7696	0.83
	$S_0 \rightarrow T_1$	577 [2.14]	-	
Dimethyl sulfoxide	$S_0 \rightarrow S_1$	417 [2.97]	0.7820	0.82
	$S_0 \rightarrow T_1$	575 [2.15]		

BBPDQ molecule with two closest neighbor dipoles (from crystal structure)

Dipole moment of the molecule was obtained from a single point calculation (B3LYP/6-31G(d)) using the geometry from the crystal structure; the value is found to be 18.1088 D. Based on the length of the dipole (assumed to be along the diaminomethylene carbon – dicyanomethylene carbon atom, r = 5.718 Å), the charge on these atoms can be determined to be +0.66e and -0.66e respectively (Fig. S14a). The local field around the BBPDQ molecule in the crystalline environment is modeled using the neighboring dipoles.[S4] In the present calculation, the two closest ones positioned based on the molecular assembly in the crystal were used (Fig. S14b); the excitation energy ($S_0 \rightarrow S_1$) was computed (TD-DFT/B3LYP/6-31G(d)). In order to mimic the environment in the amorphous state, the neighboring dipoles were moved by small distances. Computations show decrease in the excitation energy; when the distance is increased by 10% from the central BBPDQ molecule (Fig. S14c), the computed excitation energy is found to be in good agreement with the observed value. The results are listed in Table S7.
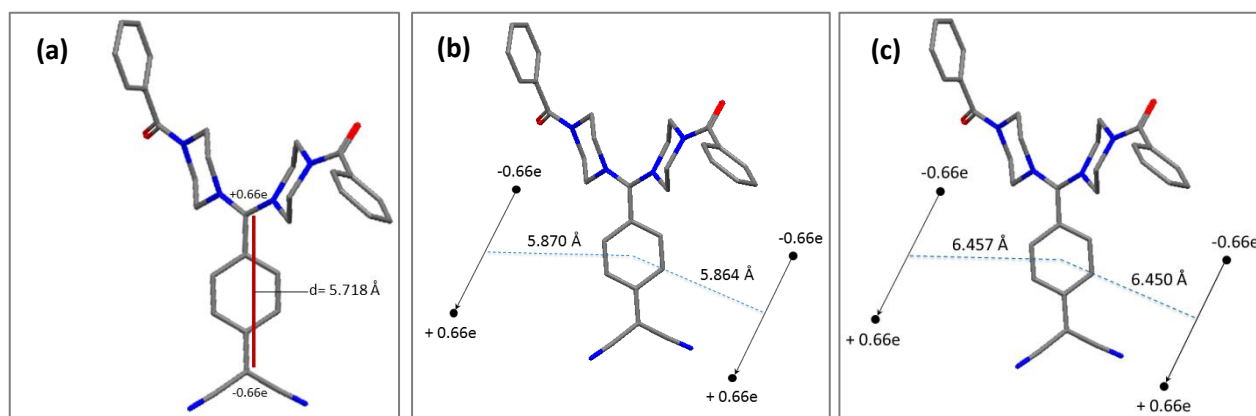

Figure S14. (a) BBPDQ molecule showing the computed dipole charges. BBPDQ molecule with the closest neighboring dipoles, **(b)** as in the crystal structure, and **(c)** moved away by 10%; the black dots indicate the point charges and the arrow, the dipole orientation.

Table S7. Experimental absorption energies of BBPDQ in the crystalline and amorphous forms compared with the values from the computational modeling.

|	Experiment	Calculation	
Form	λ_{max} (nm)	λ_{max} (nm) [osc. strength]	Model
Crystalline	430	435 [2.85]	Fig. S14b
Amorphous	440	444 [2.79]	Fig. S14c

Studies on 7,7-bis(*N*-phenylpiperazino)-8,8-dicyanoquinodimethane (BPPDQ)
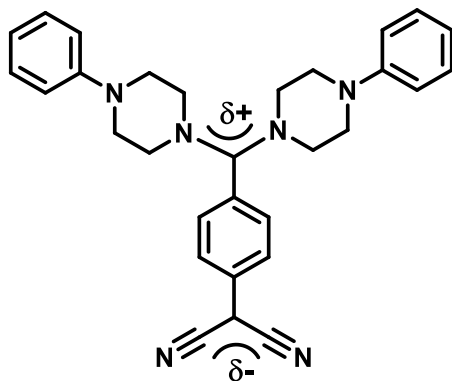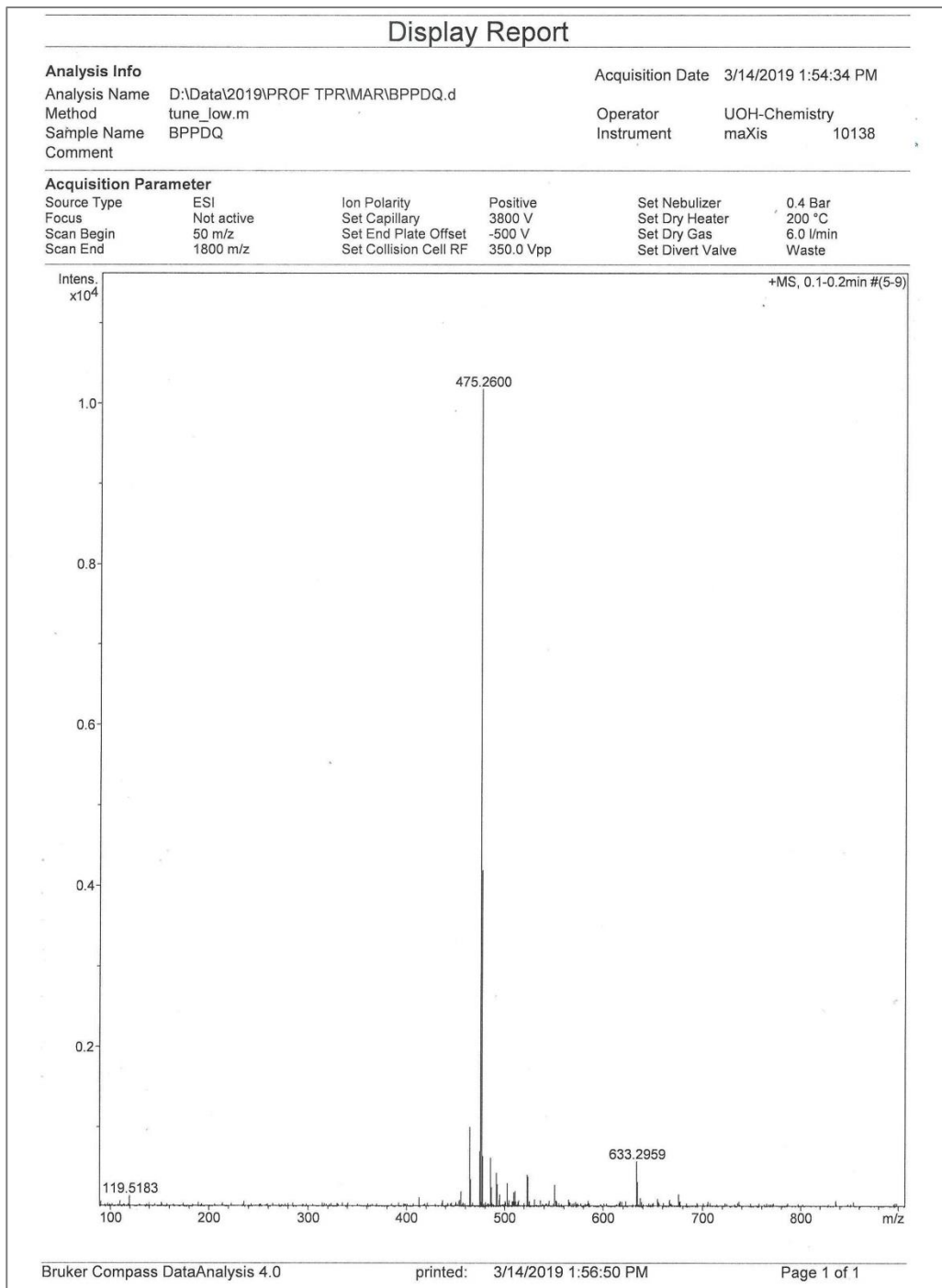

BPPDQ

Synthesis and characterization:

Same procedure as used for the preparation of BBPDQ was employed, with TCNQ (0.5 g, 2.45 mmol), 1-phenylpiperazine (1g, 6.12 mmol) and acetonitrile (30 ml). Yield of BPPDQ = 85%; FTIR : $\bar{\nu}$ /cm^{-1} = 2824.6, 2172.9, 2137.3, 1591.3, 1555.9; ^{1}H NMR (500 MHz, d$_6$-DMSO, 25°C): δ/ppm = 7.41 (d, *J*= 8.5 Hz, 2H), 7.28-7.25 (m, 4H), 7.00 (d, *J*= 8.0 Hz, 4H), 6.89 (d, *J*= 8.35 Hz, 2H), 6.83 (t, J= 7.30 Hz, 2H), 3.84 (br, 4H), 3.43 (br, 8H), 3.35 (br, 4H); ^{13}C-NMR (100 MHz, d$_6$-DMSO, 25°C): δ/ppm = 169.1, 150.9, 150.2, 132.5, 132.4, 129.6, 123.5, 120.1, 118.5, 116.5, 114.3, 51.1, 49.1; HRMS (ESI-TOF): calculated for C$_{30}$H$_{30}$N$_6$, 474.2532 Da; observed, 475.2600 Da (M + H$^+$).
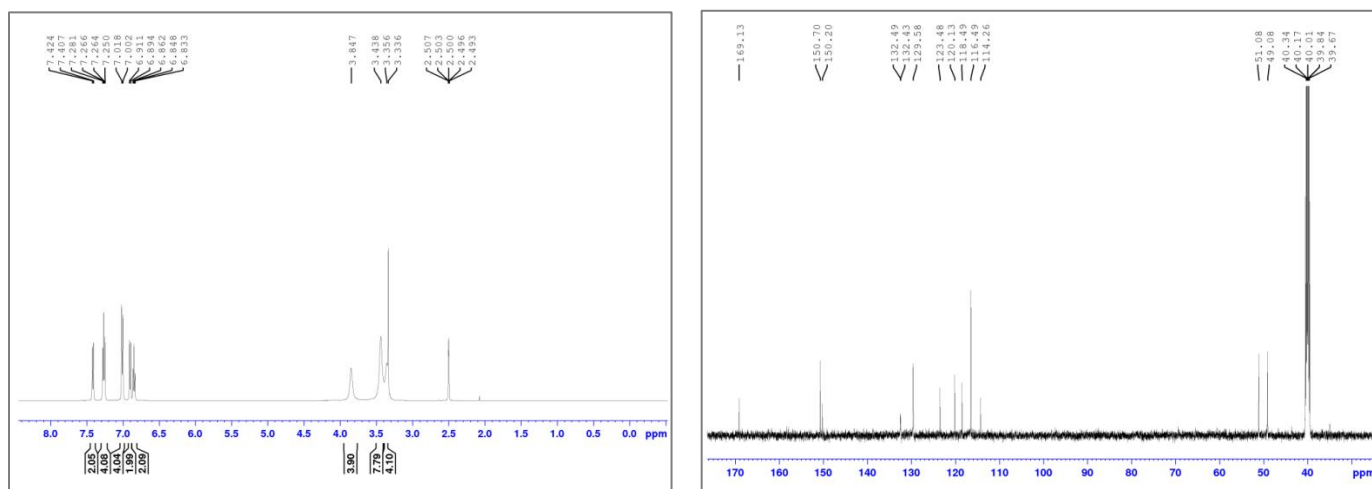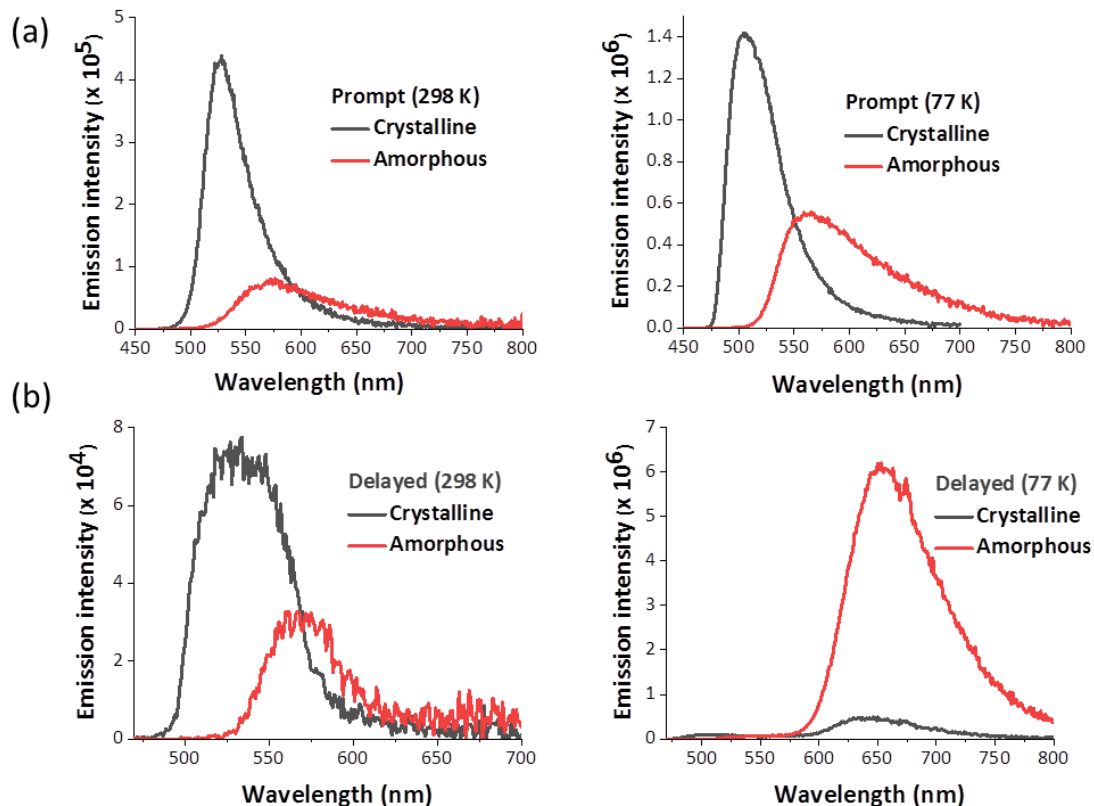

Figure S15. ^{1}H and ^{13}C NMR spectra of BPPDQ.

**Figure S16.** High resolution mass spectrum of BPPDQ.

Spectral studies:

Figure S17. Comparison of the **(a)** fluorescence and **(b)** phosphorescence responses of crystalline and amorphous samples of BPPDQ with optical density adjusted to be the same (λ_{exc} = 350 nm), at different temperatures.

Table S8: Emission lifetimes (individual components and average values) for crystalline sample of **BPPDQ** at 298 K and 77 K [λ_{exc} = 350 nm for emission spectral measurements and 330 (nano-LED) for TCSPC measurements].

	λ_{em} (nm)	τ_1 (A_1)	τ_2 (A_2)	Mean lifetime	χ^2
298 K					
Prompt	525	0.90 ns (81 %)	3.02 ns (19 %)	1.30 ns	1.06
Delayed	525	5.16 μs (78%)	10.34 μs (22%)	6.30 μs	1.09
77 K					
Prompt	504	1.32 ns (73 %)	2.99 ns (27%)	1.77 ns	1.21
Delayed	504	5.44 μs (54%)	57.98 μs (46%)	29.60 μs	1.15
	640	727.22 ms (100 %)	-	727.22 ms	1.28
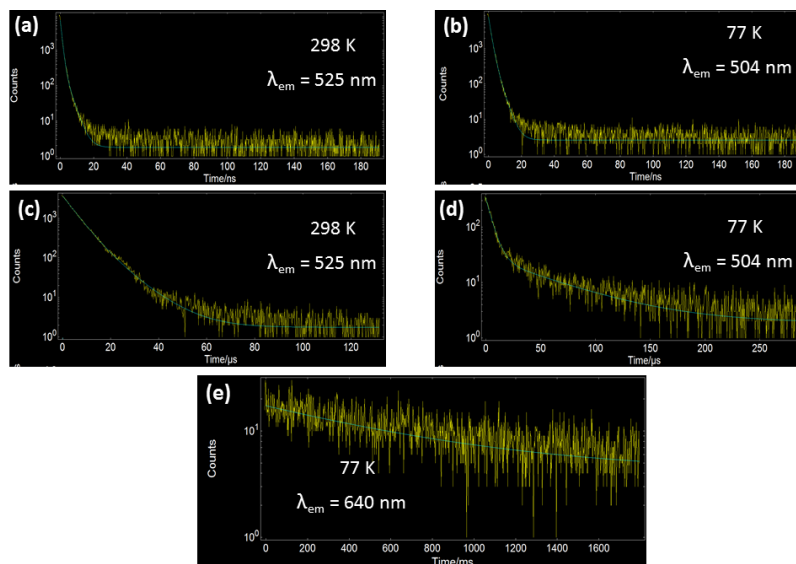
Figure S18. Prompt fluorescence decay profiles of crystalline BPPDQ at **(a)** 298 K and **(b)** 77 K; the fitting curves are shown. Delayed emission decay profiles of crystalline BPPDQ at **(c)** 298 K, **(d)** 77 K (at λ_{em} = 504 nm) and **(e)** 77 K (at λ_{em} = 640 nm) ; the fitting curves are shown.

Table S9. Emission lifetimes (individual components and average values) for amorphous sample of **BPPDQ** at 298 K and 77 K [λ_{exc} = 350 nm for emission spectral measurements and 330 (nano-LED) for TCSPC measurements].
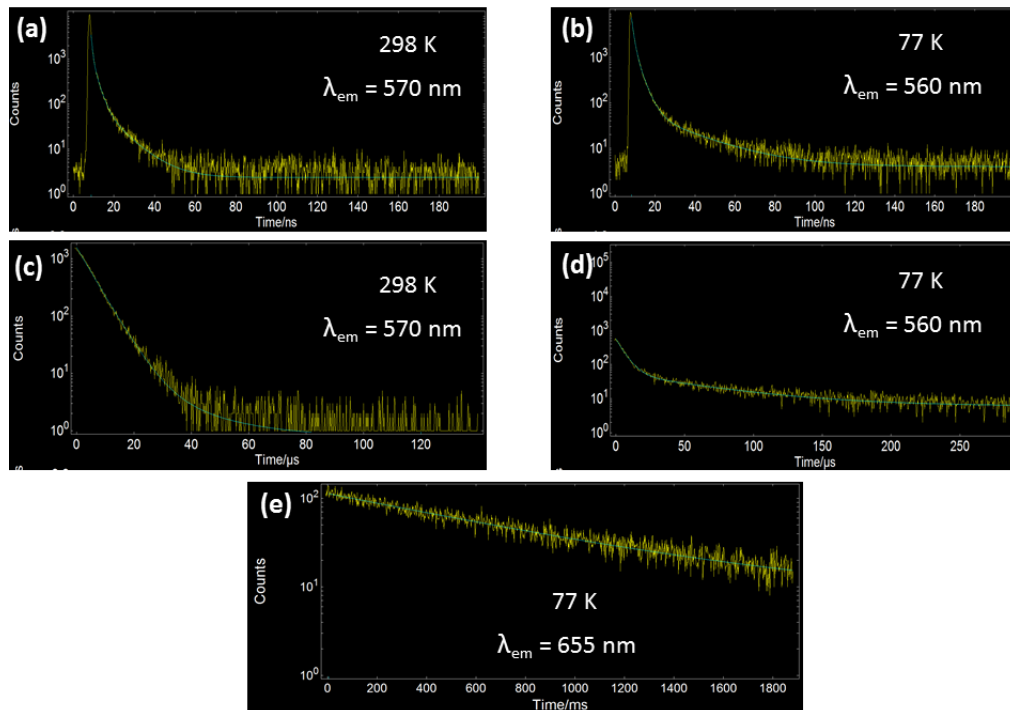
	λ_{em} (nm)	τ_1 (A$_1$)	τ_2 (A$_1$)	τ_3 (A$_3$)	Mean lifetime	χ^2
298 K						
Prompt	570	0.59 ns (32 %)	2.46 ns (49 %)	9.99 ns (19 %)	3.29 ns	1.11
Delayed	570	5.07 µs (97%)	18.01 µs (3 %)		5.45 µs	0.97
77 K						
Prompt	560	1.00 ns (43 %)	3.25 ns (47%)	22.98 ns (10)	4.25 ns	1.08
Delayed	560	5.90 µs (51 %)	60.63 µs (49)	-	32.72 µs	1.09
	655	740.55 ms (100 %)	-	-	740.55 ms	1.10

Figure S19. Prompt fluorescence decay profiles of crystalline BPPDQ at **(a)** 298 K and **(b)** 77 K; the fitting curves are shown. Delayed emission decay profiles of crystalline BPPDQ at **(c)** 298 K (at λ_{em} = 570 nm), **(d)** 77 K (at λ_{em} = 560 nm) and **(e)** 77 K (at λ_{em} = 655 nm) ; the fitting curves are shown.

Table S10. Emission characteristics of crystalline and amorphous BPPDQ: λ_{max}, mean lifetime and intensity (for samples with matched optical density).

Temperature (K)	Emission	Crystalline			Amorphous		
		λ_{max} (nm)	Mean lifetime	Intensity (10^5 au)	λ_{max} (nm)	Mean lifetime	Intensity (10^5 au)
77	Prompt	504	1.77 ns	14.2	560	4.25 ns	5.5
	Delayed	504	29.60 µs	0.9	560	32.72 µs	0.8
		640	727.22 ms	4.9	655	740.55 ms	60.5
298	Prompt	525	1.30 ns	4.3	570	3.29 ns	0.8
	Delayed	525	6.30 µs	0.7	570	5.45 µs	0.3

Table S11. The singlet-triplet ($S_1 \rightarrow T_1$) gap, ΔE_{ST} determined from the prompt and delayed emissions at 77K for BPPDQ.

Form	Transition	λ_{max}(nm) [eV]	ΔE_{ST} (eV)
Crystalline	$S_1 \rightarrow S_0$	504 [2.46]	0.52
	$T_1 \rightarrow S_0$	640 [1.94]	
Amorphous	$S_1 \rightarrow S_0$	560 [2.21]	0.32
	$T_1 \rightarrow S_0$	655 [1.89]	

References

S1 a) SAINT-NT, Version 6.04; Bruker AXS: Madison, WI, 2001; b) SHELXTL-NT, Version 6.10; Bruker AXS: Madison, WI, 2000.

S2 a) A. D. Becke, *J. Chem. Phys.* 1993, **98**, 5648; b) M. J. Frisch, G. W. Trucks, H. B. Schlegel, G. E. Scuseria, M. A. Robb, J. R. Cheeseman, G. Scalmani, V. Barone, B. Mennucci, G. A. Petersson, H. Nakatsuji, M. Caricato, X. Li, H. P. Hratchian, A. F. Izmaylov, J. Bloino, G. Zheng, J. L. Sonnenberg, M. Hada, M. Ehara, K. Toyota, R. Fukuda, J. Hasegawa, M. Ishida, T. Nakajima, Y. Honda, O. Kitao, H. Nakai, T. Vreven, J. A. Montgomery, Jr., J. E. Peralta, F. Ogliaro, M. Bearpark, J. J. Heyd, E. Brothers, K. N. Kudin, V. N. Staroverov, R. Kobayashi, J. Normand, K. Raghavachari, A. Rendell, J. C. Burant, S. S. Iyengar, J. Tomasi, M. Cossi, N. Rega, J. M. Millam, M. Klene, J. E. Knox, J. B. Cross, V. Bakken, C. Adamo, J. Jaramillo, R. Gomperts, R. E. Stratmann, O. Yazyev, A. J. Austin, R. Cammi, C. Pomelli, J. W. Ochterski, R. L. Martin, K. Morokuma, V. G. Zakrzewski, G. A. Voth, P. Salvador, J. J. Dannenberg, S. Dapprich, A. D. Daniels, O. Farkas, J. B. Foresman, J. V. Ortiz, J. Cioslowski and D. J. Fox, Gaussian 09, Revision A.02, Gaussian, Inc., Wallingford, CT, 2009; c) A. D. Becke, *Phys. Rev. A.* 1988, **38**, 3098; d) C. Lee, W. Yang and R. G. Parr, *Phys. Rev. B.* 1988, **37**, 785.

S3 a) S. Jayanty, T. P. Radhakrishnan, *Chem. Mater.* 2001, **13**, 2460; b) P. Srujana, T. P. Radhakrishnan, *J. Mater. Chem. C* 2016, **4**, 6510; c) P. Srujana, T. P. Radhakrishnan, *Chem. Eur. J.* 2018, **24**, 1784.

S4 P. Srujana, T. P. Radhakrishnan, *Angew. Chem. Int. Ed.*, 2015, **54**, 7270.